View metadata, citation and similar papers at core.ac.uk
brought to you by CORE
provided by Elsevier - Publisher Connector

subchondral bone plate in the center of the medial and lateral condyles and two ROIs (~ 14 mm x 14 mm) immediately below the subchondral bone plate in the trabecular bone. Anatomical landmarks for the ROIs were tibial spine, subchondral bone plate, and outer borders of the proximal tibia. A custom-made MATLAB software (MathWorks Inc., USA) was used for the manual placement of the ROIs. For the μCT data, the ROIs were placed in the 2D coronal projection image from the μCT slices. After that, ROIs were extracted from every slice of the μCT stack separately. These μCT data (3D ROIs) were then evaluated using SkyScan CTAn software (Bruker, Belgium). From the plain radiographs, mean grayscale value of the ROI (GV) and aluminum step wedge thickness that corresponds to the measured GV (GV_{mmAl}) were calculated to evaluate bone density. To evaluate bone structure, local binary patterns (LBP) operator was applied to the radiographs after median filtering (3x3 pixels). From the generated LBP image, entropy (E_{LBP}) was calculated. From the μCT 3D ROIs, conventional 3D parameters were calculated: bone volume fraction (BV/TV), bone surface density (BS/TV), trabecular thickness (Tb.Th), trabecular separation (Tb.Sp), trabecular number (Tb.N), fractal dimension (FD), Euler number (Eu.N), and connectivity density (Conn.Dn). Furthermore, to simulate plain radiography, every μCT slice was binarized and summed together to construct 2D coronal projection image from the 3D μCT data. From this projection image, GV and E_{LBP} were calculated similarly as from the plain radiographs.To evaluate relationship between different parameters, Pearson (r) correlation analysis was applied using IBM SPSS 22 software (IBM SPSS, USA).

Results: Correlation coefficients between 3D μCT parameters and parameters from the plain radiograph and from the μCT projection image with all ROIs pooled together ($n = 44$) are shown in the Table 1. Strong correlations between GV_{mmAl} from the plain radiograph and BV/TV ($r = 0.86$, $p < 0.01$), and between GV from the μCT 2D projection image and BV/TV ($r = 0.93$, $p < 0.01$) were observed (Figure 1). Furthermore, correlations between Conn.Dn and E_{LBP} from both the plain radiograph ($r = 0.58$, $p < 0.01$) and the μCT 2D projection image ($r = 0.73$, $p < 0.01$) are shown in the Figure 1. Correlation between Eu.N and parameters from the plain radiograph and the 2D projection image from μCT were higher when subchondral and trabecular bone ROIs were not pooled together (Table 2).

Conclusions: Current results indicate that estimates for both the subchondral bone density (amount of bone within a volume) and structure, evaluated from 2D plain radiographs, are significantly related with the corresponding 3D μCT measures. Correlation between bone density estimated from plain radiograph and BV/TV was higher after the grayscale values in plain radiograph were calibrated to the aluminum step wedge in image (GV_{mmAl}) than without calibration (GV). However, it should be noted that in this *in vitro* study the bones were not surrounded with soft tissue, and therefore error/noise resulting from soft tissue was not present in the measurements. E_{LBP} seemed to correlate better with connectivity measures (Eu.N and Conn.Dn) than the bone density-related parameters did. Since Eu.N is dependent on the ROI size, results were also shown for both subchondral and trabecular bone ROIs separately.

Table 1
Pearson correlation coefficients between 3D μCT parameters and parameters from 2D plain radiographs and 2D projection image from μCT. All ROIs pooled together ($n = 44$).

μCT parameter	Plain radiograph			2D projection image from μCT	
	GV	GV_{mmAl}	E_{LBP}	GV	E_{LBP}
BV/TV	0.77**	0.86**	0.36*	0.93**	0.71**
BS/TV	0.65**	0.78**	0.51**	0.86**	0.80**
Tb.Th	0.70**	0.72**	0.05	0.73**	0.41*
Tb.Sp	-0.58**	-0.70**	-0.51**	-0.79**	-0.77**
Tb.N	0.64**	0.76**	0.51**	0.87**	0.80**
FD	0.62**	0.75**	0.48**	0.87**	0.84**
Eu.N	0.25	0.16	-0.20	0.09	-0.22
Conn.Dn	0.44**	0.58**	0.58**	0.64**	0.73**

**$p < 0.01$, *$p < 0.05$

Table 2
Pearson correlation coefficients between Eu.N and parameters from 2D plain radiographs and 2D projection image from μCT separately for subchondral ($n = 22$) and trabecular bone ROIs ($n = 22$).

	Plain radiograph			2D projection image from μCI	
	GV	GV_{mmA1}	E_{LBP}	GV	E_{LBP}
Subchondral bone:					
Eu.N	-0.34	-0.50*	-0.58**	-0.57**	-0.76**
Trabecular bone:					
Eu.N	-0.32	-0.52*	-0.61**	-0.61**	-0.76**

**$p<0.01$, *$p < 0.05$.

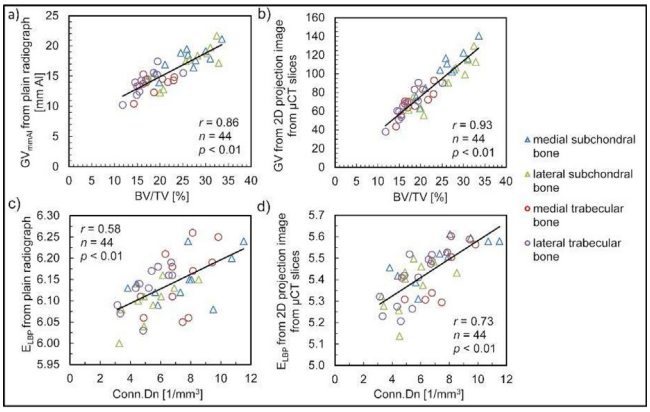

Figure 1a) Correlations between GV_{mmA1} from plain radiographs and BV/TV, b) between GV from 2D projection image from μCT slices and BV/TV, c) between H_{LBP} from plain radiograph and connection density (Conn.Dn), and d) between E_{LBP} from 2D projection image from μCT sliccs and Conn.Dn.

368
CORRELATION OF NON-DESTRUCTIVE ELECTROMECHANICAL PROBE (ARTHRO-BST) ASSESSMENT WITH HISTOLOGICAL SCORES AND MECHANICAL PROPERTIES IN HUMAN TIBIAL PLATEAU

S. Sim †‡, A. Chevrier †, M. Garon ‡, E. Quenneville ‡, M.D. Buschmann †.
† *Polytechnique Montréal, Montréal, QC, Canada;* ‡ *Biomomentum Inc., Laval, QC, Canada*

Purpose: The purpose of the current study is to investigate whether electromechanical properties of articular cartilage in human tibial plateau correlated with histological scores and unconfined compression parameters as in human distal femurs (Sim et al., 2014).

Methods: Right and left tibial plateaus from six human donors (5 males and 1 female, average age 48 years) were provided by RTI Surgical (Alachua, FL, USA). *Ex vivo* mappings of electromechanical properties of entire articular surfaces were performed using the Arthro-BST. The device calculates a quantitative parameter (QP) of cartilage electromechanical activity corresponding to the number of microelectrodes in contact with the cartilage when the sum of their streaming potential reaches 100 mV. A high QP indicates weak electromechanical properties and vice-versa. Subsequently, osteochondral cores were harvested from normal and visually abnormal regions on the tibial plateau. A total of 56 cores were tested in unconfined compression to obtain the fibril modulus (Ef), equilibrium modulus (Em), and permeability (k) prior to histoprocessing. Safranin O-Fast Green-stained paraffin sections were scored with the Mankin histological-histochemical grading system. The electromechanical QP corresponding to each cored site was calculated as the average of all QPs measured within 6 mm from the core center location.

Results: As the electromechanical QP increases, safranin O/Fast Green stained sections showed that GAG staining in the cartilage matrix and structural integrity decreases (Fig. 1). A strong correlation was found between electromechanical QP and Mankin score ($r = 0.50$, $p = 0.0004$). A strong correlation was also found between QP and Ef ($r = -0.73$, $p < 0.0001$; Fig. 2A) and QP and permeability (log k) ($r = 0.64$, $p < 0.0001$;

Fig. 2B). Weak correlations were found between QP and Em ($r = -0.30$, $p = 0.0186$; Fig. 2C) and between QP and thickness of the articular cartilage ($r = 0.42$, $p = 0.0006$; Fig. 2D). As expected, the electromechanical QP decreases with increasing Ef and Em whereas the electromechanical QP increases with Mankin Score, permeability and thickness.

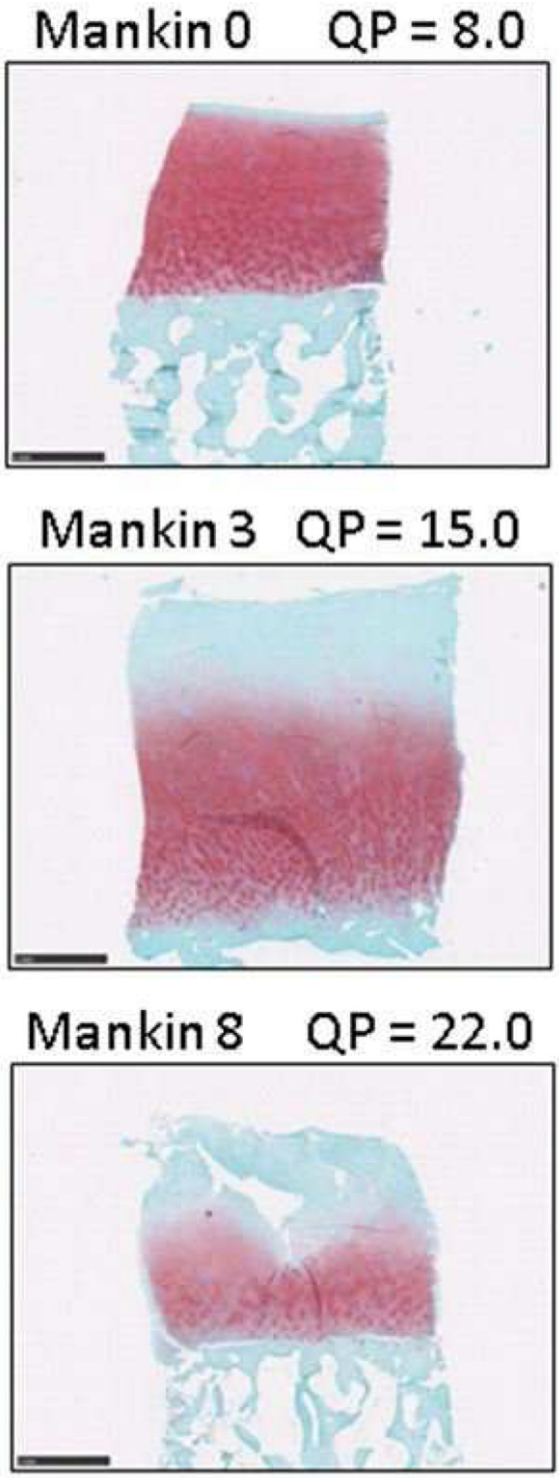

Figure 1. Representative Safranin O/Fast Green stained sections for 3 Mankin scores and their corresponding electromechanical QP; Bars = 1 mm.

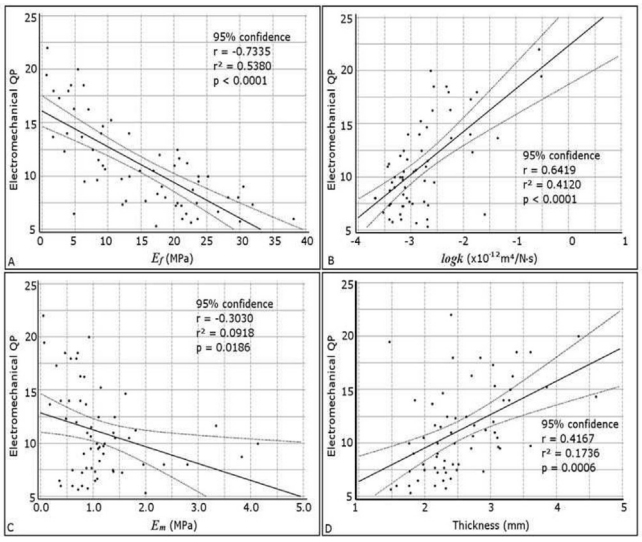

Figure 2(A) Correlation between the electromechanical QP and fibril modulus E_f. (B) Correlation between the electromechanical QP and permeability *logk*; (C) Correlation between the electromechanical QP and matrix modulus E_m; (D) Correlation between the electromechanical QP and cartilage thickness.

Conclusions: The electromechanical QP measured in human tibial plateau correlated significantly with the histological Mankin score and with unconfined compression mechanical parameters, similar to what was previously seen in human distal femurs. Moreover, a weak correlation was found between the thickness of the cartilage on the tibial plateau and the electromechanical QP. This is in contrast to what was previously observed in the distal femurs but could be related to topographical variations present on the tibial plateau surface, where cartilage is very thin and rigid in regions covered by the meniscus but thicker and softer in regions not covered by meniscus. Considering these results, we believe that the Arthro-BST can provide a reliable tool for articular cartilage assessment on human tibial plateau.

369
DEMOGRAPHIC AND BIOMECHANICAL FACTORS RELATED TO STRUCTURAL PROGRESSION OF HIP OSTEOARTHRITIS OVER 18 MONTHS

D. Kumar †, C. Wyatt ‡, N. Okazaki ‡, K. Chiba §, S. Lee ‡, T.M. Link ‡, R.B. Souza ‡, S. Majumdar ‡. † *Med. Univ. of South Carolina, Charleston, SC, USA;* ‡ *Univ. of California, San Francisco, San Francisco, CA, USA;* § *Nagasaki Univ. Sch. of Med., Nagasaki, Japan*

Purpose: Unlike knee osteoarthritis (OA), factors related to hip OA progression are not well understood. A major reason has been a lack of longitudinal studies in hip OA using MRI to quantify progression. The goals of this study were (a) to evaluate the natural evolution of hip cartilage lesions, labral tears, bone marrow lesions (BML) and subchondral cysts over 18 months in individuals with and without mild-moderate radiographic hip OA, and (b) to investigate demographic (age, sex, BMI) and biomechanical (sagittal hip kinematics during walking) factors that may be related to the progression of hip OA related MR parameters.

Methods: Fifty-seven subjects with radiographic hip OA (+ROA, Kellgren-Lawrence = 2,3; n = 19, Age = 54.6±2.6 years; BMI = 24.0±2.6 kg/m^2, 12 Men: 7 Women) and without radiographic hip OA (-ROA, Kellgren-Lawrence = 0,1; n = 38, Age = 43.3±12.8 years; BMI = 23.7±3.2 kg/m^2, 19 Men: 19 Women) were imaged using a 3.0 Tesla MRI scanner (MR GE 750) at baseline and 18 months. Cartilage lesions, BML, cysts, and labral tears were graded using a semi-quantitative MRI score (Scoring Hip Osteoarthritis with MRI – SHOMRI). Other parameters analyzed included posterior wall sign, cross-over sign, and center edge angle from radiographs, alpha angle from oblique axial MRI, and patient-reported Hip disability and Osteoarthritis Outcome Score (HOOS). Subjects were classified as progressors or non-progressors based on an increase in any MRI OA parameter (increase in either cartilage, labrum, BML, or cyst scores). Fisher's Exact Test was used to